Journal of Power Sources 196 (2011) 10563–10569

Contents lists available at SciVerse ScienceDirect

Journal of Power Sources

journal homepage: www.elsevier.com/locate/jpowsour

Nano mineral fiber enhanced catalyst coated membranes for improving polymer electrolyte membrane fuel cell durability

Feng Xu, Ran Xu, Shichun Mu*

State Key Laboratory of Advanced Technology for Materials Synthesis and Processing, Wuhan University of Technology, Wuhan 430070, PR China

ARTICLE INFO

Article history:
Received 1 July 2011
Received in revised form 22 August 2011
Accepted 23 August 2011
Available online 30 August 2011

Keywords:
Palygorskite
Catalyst coated membrane
Chemical stability
Mechanical stability
Polymer electrolyte membrane fuel cell

ABSTRACT

In order to protect the perfluorosulfonic acid (PFSA) ionomer from an attack of contaminant metal ions as well as to enhance the mechanical stability of catalyst layers, palygorskite (PGS) is introduced into the catalyst layer of polymer electrolyte membrane fuel cells. PGS is a widely used natural nano-sized silicate mineral fiber with unique nano-sized channel structure, has a strong absorption capacity for heavy metal ions. We identify a negative influence of Fe^{2+} on PFSA membranes to make a comparative study. Subsequently catalyst coated membranes (CCMs) prepared with a PGS-Pt/C composite catalyst show a great effect in reducing Fe^{2+} ion crossover. Results display that PGS absorbs Fe^{2+} in nano-structure channels, and effectively protect PFSA ionomer in both the catalyst layer and membrane from hydroxyl radicals ($OH^{\bullet}$) attack. Thus, the chemical stability of PFSA ionomer in both the catalyst layer and membrane is greatly improved. Furthermore, the enhancement of the mechanical performance of catalyst layers is discussed.

1. Introduction

Increasing the durability of catalyst coated membranes (CCMs) used in polymer electrolyte membrane fuel cells (PEMFCs) remains a major challenge and a growing research focus [1]. PEMFCs work under extremely harsh conditions: low pH (<1), high humidity, wide temperature range (−40 °C to 80 °C or above), high electrochemical potential (from 0.6 to 1.2 V vs. reversible hydrogen electrode, RHE), strongly reducing atmosphere at anode (H_2) and radical oxidization condition at the cathode (O_2) [2–4]. In these cases, the CCM component suffers severe degradations. Metal ions (Fe^{2+}, Cu^{2+}, Cr^{3+}, etc.) produce hydroxyl radicals ($OH^{\bullet}$) in electrochemical system. The proposed reactions are as follows [5,6]:

$$H_2O_2 + Fe^{2+} \rightarrow Fe^{3+} + HO^- + OH^{\bullet} \quad (I)$$

$$R_f\text{–}CF_2COOH + OH^{\bullet} \rightarrow R_f\text{–}CF_2^{\bullet} + CO_2 + H_2O \quad (II)$$

$$R_f\text{–}CF_2^{\bullet} + OH^{\bullet} \rightarrow R_f\text{–}CF_2OH \rightarrow R_f\text{–}COF + HF \quad (III)$$

$$R_f\text{–}COF + H_2O \rightarrow R_f\text{–}COOH + HF \quad (IV)$$

The resultant $OH^{\bullet}$ attacks the per-fluorocarbon backbone and side-chain groups, leading to the degradation of perfluorosulfonic acid (PFSA) electrolyte in both the membrane and catalyst layer. Subsequently, declines of both the mechanical strength and proton conductivity occur, resulting in an increase in total cell resistance and loss of output power capability [1,7].

Besides the chemical degradation of PFSA electrolyte, the mechanical damages to CCMs also play an important role in the degradation of fuel cell performance [8]. They appear as micro-cracks, delamination, pinholes, and debonding between the electrolyte and the catalyst [9–11], which cause the loss of catalysts and the dissolution or decomposition of PFSA electrolyte. According to our previous work, the damage to the catalyst layer can lead to an exposure of membranes which are readily attacked by OH radicals, promoting the formation of micro-cracks or pinholes, causing the failure of the fuel cell due to severe hydrogen crossover [9,10].

In order to prevent the degradation of CCMs we introduce for the first time a natural mineral fiber – palygorskite (PGS) into the catalyst layer to absorb the contaminant metal ions as well as to enhance the mechanical property of catalyst layers. PGS has attracted extensive attentions as a reinforcement agent for enhancing the matrix performance in mechanical, electrical and optical properties and in water retention property [12–14]. Its unique properties, such as high surface area, high absorption capacity, elongate, and especially nano-fiber structure, have been characterized and applied. The idealized unit cell formula of PGS is $M_{(x+y+2z/2)}^{2+}{\cdot}nH_2O[Mg_{5-y-z}R_{y\square z}](Si_{8-x}R_x)O_{20}(OH)_2(H_2O)_4$, where R is Al (III) or Fe (III), □ is an interstitial vacancy, and M^{2+} is an exchangeable cation [15]. Its structure consists of continuous $(Si, Al)_2O_5$ sheets which are linked by octahedral ribbons (Mg, Al, Fe^{3+}). The ribbons are very sharp and chainlike to form unique nano-structural channels. H_2O molecules and some metal cations can be accommodated in these channels [16,17]. Water

* Corresponding author. Tel.: +86 27 8765 1837; fax: +86 27 8787 9468.
E-mail addresses: msc@whut.edu.cn, mushichun@gmail.com (S. Mu).

0378-7753/$ – see front matter © 2011 Elsevier B.V. All rights reserved.
doi:10.1016/j.jpowsour.2011.08.098

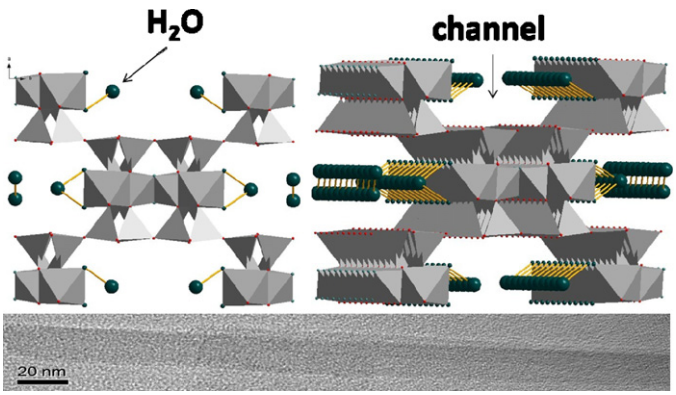

Fig. 1. Scheme and TEM image of PGS. Top-left: idealized structure projected onto (0 0 1). Top-right: the channel structure exhibited by ten cells (green balls represent H_2O, yellow lines represent bonds, gray tetrahedron represent silicon-oxygen tetrahedron). Bottom: TEM image of PGS fiber. (For interpretation of the references to color in this figure legend, the reader is referred to the web version of the article.)

contained in PGS presents in four states: (i) absorbed water on the mineral surface; (ii) zeolitic water weakly bound in the channels which would be removed below 473 K; (iii) coordinated water bound to (Mg, Al) cations, which would be lost between 523 K and 673 K, (iv) hydroxyl water (–OH), which would be lost above 673 K [18–20]. Some isomorphic substitutions in the tetrahedron sheet (such as Al^{3+} for Si^{4+}) result in the permanent negative charge, which can enhance the adsorption/absorption of metal ions on the surface or in the channel [21–24], and provide PGS with high cation exchange capacity (CEC) as shown in Fig. 1. Our previous work has demonstrated that PGS interacts with PFSA and produces "macromolecular comb" structure forming a network in the matrix, trapping matrix materials and preventing them from separation, leading to a significant enhancement in mechanical property [25]. Such advantages provide PGS benefits to the absorption of metal ions from water solution [26,27].

In this study, the PGS has been used to absorb the contaminant metal ions to prevent the PFSA ionomer from OH radical attack in both catalyst layers and membranes, and to enhance the mechanical strength of catalyst layers, improving the durability of CCMs.

2. Experimental

Nafion211 membranes (1.0 cm × 6.0 cm) were soaked in 20 ppm Fe^{2+} ($FeCl_2$) solution for different time, followed by successive treatments with 0.5 M H_2SO_4, H_2O, H_2O_2, H_2O at 80 °C for 30 min. The membranes before and after treatments were fixed on a Teflon holder. Four measuring probes made of gold coated copper were fixed through the holder contacting with the membrane at a distance of 2.0 cm. Membrane resistance (R) was calculated using an AC impedance system (Autolab PGSTAT 30, Eco Chemie B.V.) in the range of 5000–1 Hz. The proton conductivity was calculated according to Eq. (1) as follows:

$$\sigma = \frac{l}{RS} \quad (1)$$

where σ is conductivity of the membranes (S cm^{-1}), l is thickness of the membranes (cm), and S is the contact surface area of the electrode (cm^2).

PGS samples of weight 0.95 mg, 2.0 mg, 3.6 mg and 7.7 mg were mixed with 18 mg Pt/C (60 wt%, Jonson Matthey), respectively. Then 3 mL deionized water was added, following the addition of 300 μl Nafion solution (5 wt%, Du pont). After ultrasonicating for 10 min, the catalyst inks containing 5 wt%, 10 wt%, 20 wt%, and 30 wt% PGS were prepared. Meanwhile, the catalyst ink without PGS was prepared using the same method to serve as a benchmark. The PGS used here is purchased from Guanshan, Anhui, with the CEC of 97.383×10^{-5} mol g^{-1}. The unit cell formula is $(Mg_{3.43}Al_{0.68}Fe_{0.27}Ti_{0.04\square 0.58})_{5.00}(Na_{0.00}K_{0.05}Ca_{0.01}Ba_{0.05})(Si_{7.83}Al_{0.17})_{8.00}O_{20}(OH)_2{\cdot}8H_2O$ [28].

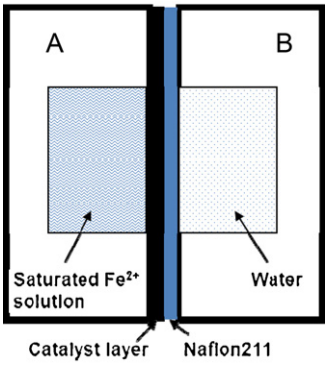

Scheme 1. Sketch of Fe^{2+} ions crossover tests.

The catalyst ink was coated onto Poly Tetra Fluorethylene (PTFE) membranes to form catalyst layers, and then transferred onto both sides of a polymer electrolyte membrane (PEM) by hot-pressing at 90 atm, 100 °C for 90 s. The PEM was Nafion®211 membrane (25 μm in thickness) and the total Pt loading of the fresh CCMs was 0.8 mg cm^{-2}. The CCMs with and without PGS are marked as CCM-P and CCM-N, respectively.

Half-CCM was fabricated, where the catalyst layer was coated only onto one side of PEM. The Pt loading of the half-CCMs was 0.4 mg cm^{-2}. The Half-CCMs were sandwiched between two chambers, as shown in Scheme 1. Chamber A in contact with catalyst layer was filled with Fe^{2+} solution, and chamber B in contact with PEM was filled with deionized water. After every 24 h, Fe^{2+} solution and deionized water were replaced by fresh ones and collected for quantitative component analyses by atom absorption spectrum (AAS) (GBC AVANTA M, GBC Scientific Equipment Pty Ltd., Australia).

Fresh CCMs were soaked in a solution of 100 mL 30% hydrogen peroxide (H_2O_2) with 20 ppm Fe^{2+} species (Fenton reactant) at 80 °C. After each 4 h, Fenton reactant was replaced by fresh ones. The morphologies of PGS and CCMs were observed by both TEM (JEM-2010, JEOC) equipped with an energy-dispersive X-ray spectroscopy (EDS) analyzer and SEM (H-600STEM/EDXPV9100, HITACHI), respectively. The concentrations of Fe^{2+} and fluoride emission in solution were detected by AAS tests.

The electrochemical performance of the composite catalyst was characterized with three-electrode system (AutolabPGSTAT 30, Eco Chemie B.V.). The catalyst ink was coated onto a mirror-polished glassy carbon disk electrode (f = 3 mm) as the working electrode. The electrochemical performance was carried out in 0.5 M H_2SO_4 solution at 20 ± 2 °C, H_2SO_4 solution was saturated by pure N_2 in order to expel oxygen in the solution. The saturated calomel electrode (SCE) was used as the reference electrode, and the platinum wire was used as the counter electrode.

3. Results and discussion

In order to test the influence of Fe^{2+} as a species of contaminant to PFSA membrane during fuel cell operation, we carried out AC impedance measurements using Nafion®211 membrane. As shown in Fig. 2, Nafion membrane endures a drastic increase in resistance after soaking in 20 ppm Fe^{2+} solution, which indicates a sharp decline in proton conductivity. However, the high resistance does not change with the soaking time. After a treatment with H_2SO_4, the resistance of the membrane partially recovered toward the original level. These results show that Fe^{2+} ions do have great

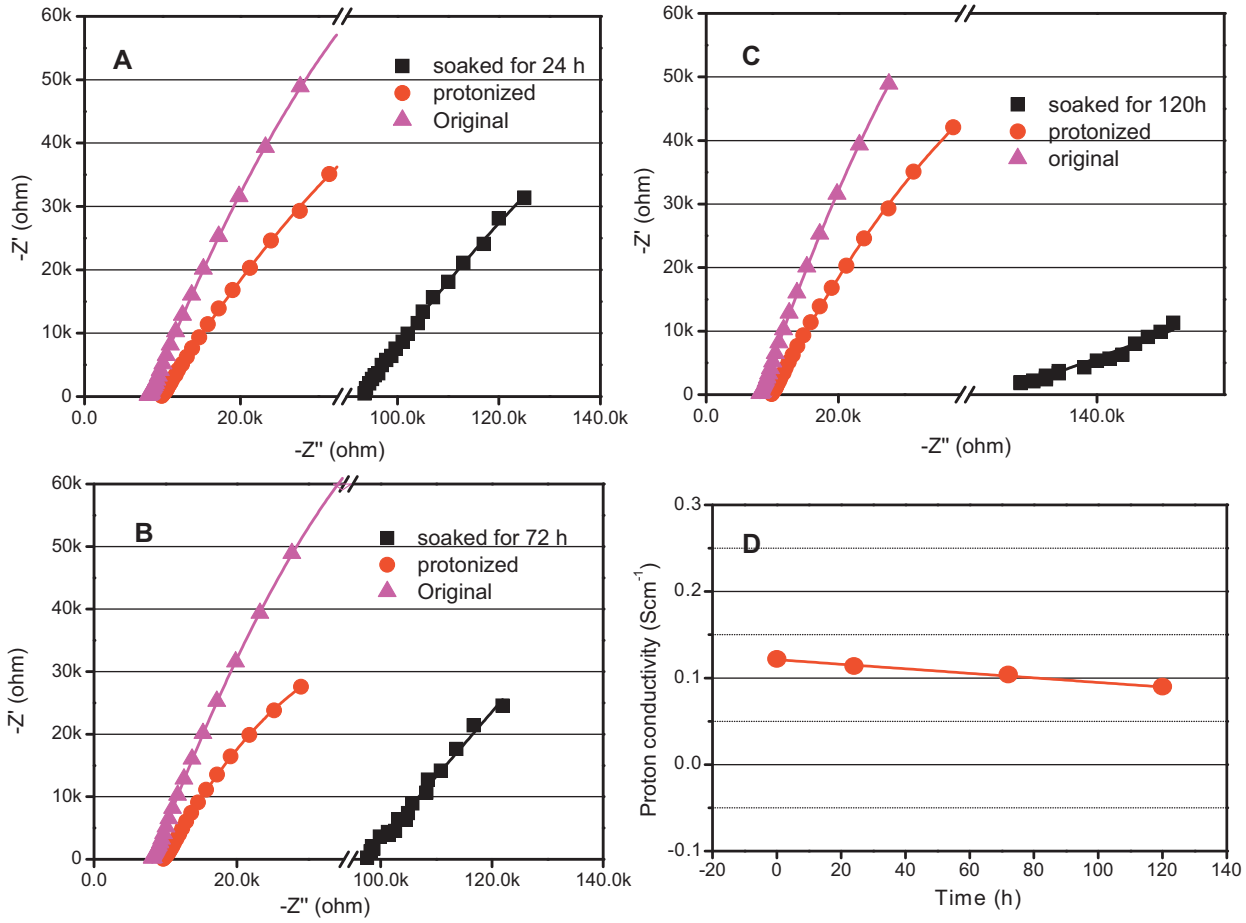

Fig. 2. Resistance of Nafion membrane after soaking for different time in Fe^{2+} solution. (A) 24 h; (B) 73 h; (C) 120 h; (D) the proton conductivity after soaking. The pink line: the AC impedance of pristine membrane; the red and black line: the AC impedance of membrane after soaking with and without treatments. The proton conductivity is extracted from the red lines in (A), (B), and (C). (For interpretation of the references to color in this figure legend, the reader is referred to the web version of the article.)

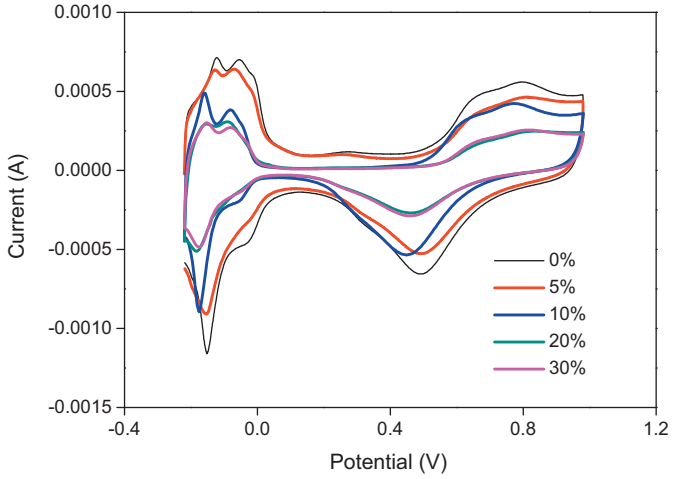

Fig. 3. CV scans of catalyst with different contents of PGS.

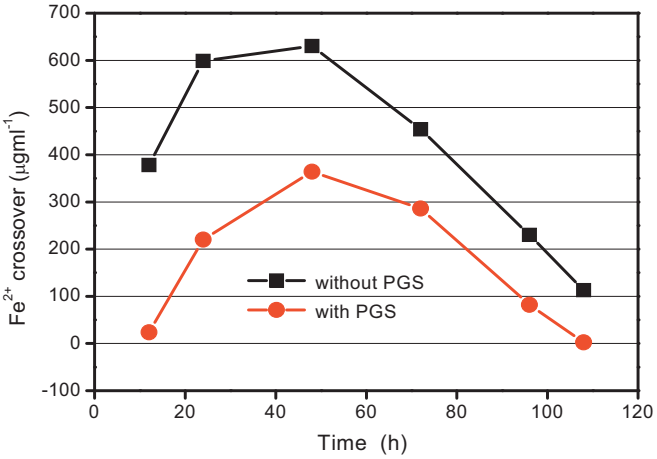

Fig. 4. Fe^{2+} ions crossover though half-CCMs.

negative influence on the performance of membrane as reported in several publications [29,30], but such influence is partially recoverable. The presence of H^+ which derives from H_2SO_4 plays an important role in this recovery. According to the cluster network model of Nafion structure, a cation migrates along the restricted path through channels of hydrophilic domains which are formed by hydrophilic exchange sites (SO_3^- end groups) [31], whether it diffuses (via pressure diffusion or normal diffusion) or is transported by electro-osmosis. The water content of the path is crucial for the membrane conductivity [32]. The heavier the cations present in the channels, the lower the hydrophilicity of the exchange site is, because the heavier cation is more tightly bound to the exchange site [33,34]. That is why the membrane endures a drastic decrease in proton conductivity after soaking in Fe^{2+} solution. H^+ is less coupled than other cations and water, making it easier to move into the membrane phase [35]. Numerous H^+ in the presence of H_2SO_4

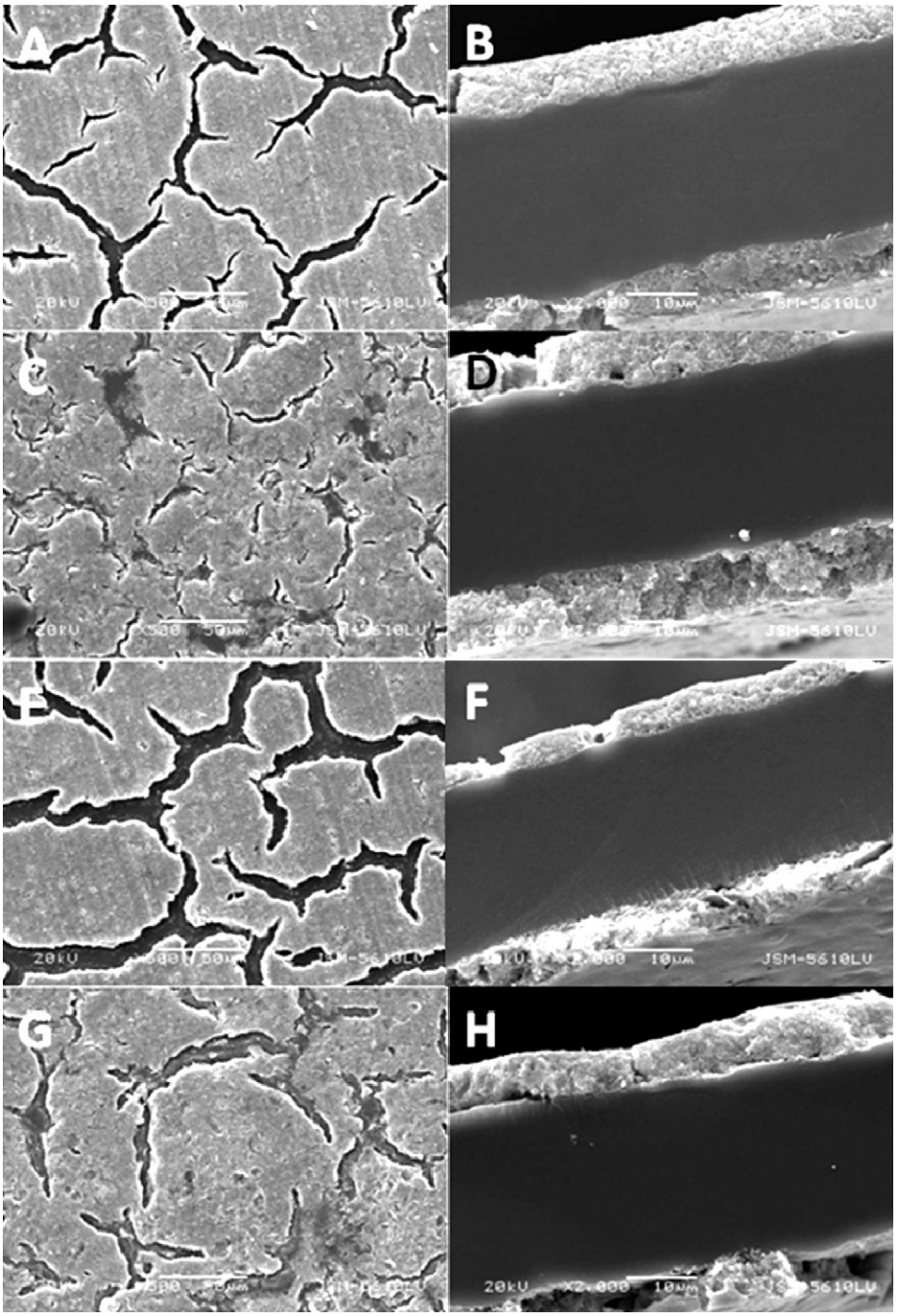

Fig. 5. SEM images of CCMs treated in Fenton's reagent after 100 h and 200 h. (A) 100 h without PGS; (C) 100 h with PGS; (E) 200 h without PGS; (G) 200 h with PGS. (B), (D), (F), and (H) are the cross-section of (A), (C), (E), and (G).

solution, flood into membrane phase to replace the Fe^{2+} which is bound to the exchange site, leading to a partially recovered property of the membrane conductivity. In fact, the oxidation reduction reactions that occur in catalyst layers under PEMFC operation are as follow:

$$\text{Anode}: H_2 \rightarrow 2H^+ + 2e^- \quad \text{(V)}$$

$$\text{Cathode}: 4H^+ + O_2 + 4e^- \rightarrow 2H_2O \quad \text{(VI)}$$

$$\text{General}: 2H_2 + O_2 \rightarrow 2H_2O \quad \text{(VII)}$$

The resultant H^+ is transported from anode to cathode through the membrane phase. This process is critical to both the PFSA ionomer and catalyst performance. Once the exchange site of the PFSA ionomer is occupied by Fe^{2+}, the transport becomes difficult to H^+, and further negatively influences the catalyst activation toward H_2 due to the absence of the effective triple-phase boundary (TPB). As a result, less H^+ are supplied to replace Fe^{2+} in the path. Such vicious circle may result in a failure of fuel cell to generate electricity. Thus, it is important to eliminate or at least decrease the negative influence of metal contaminants.

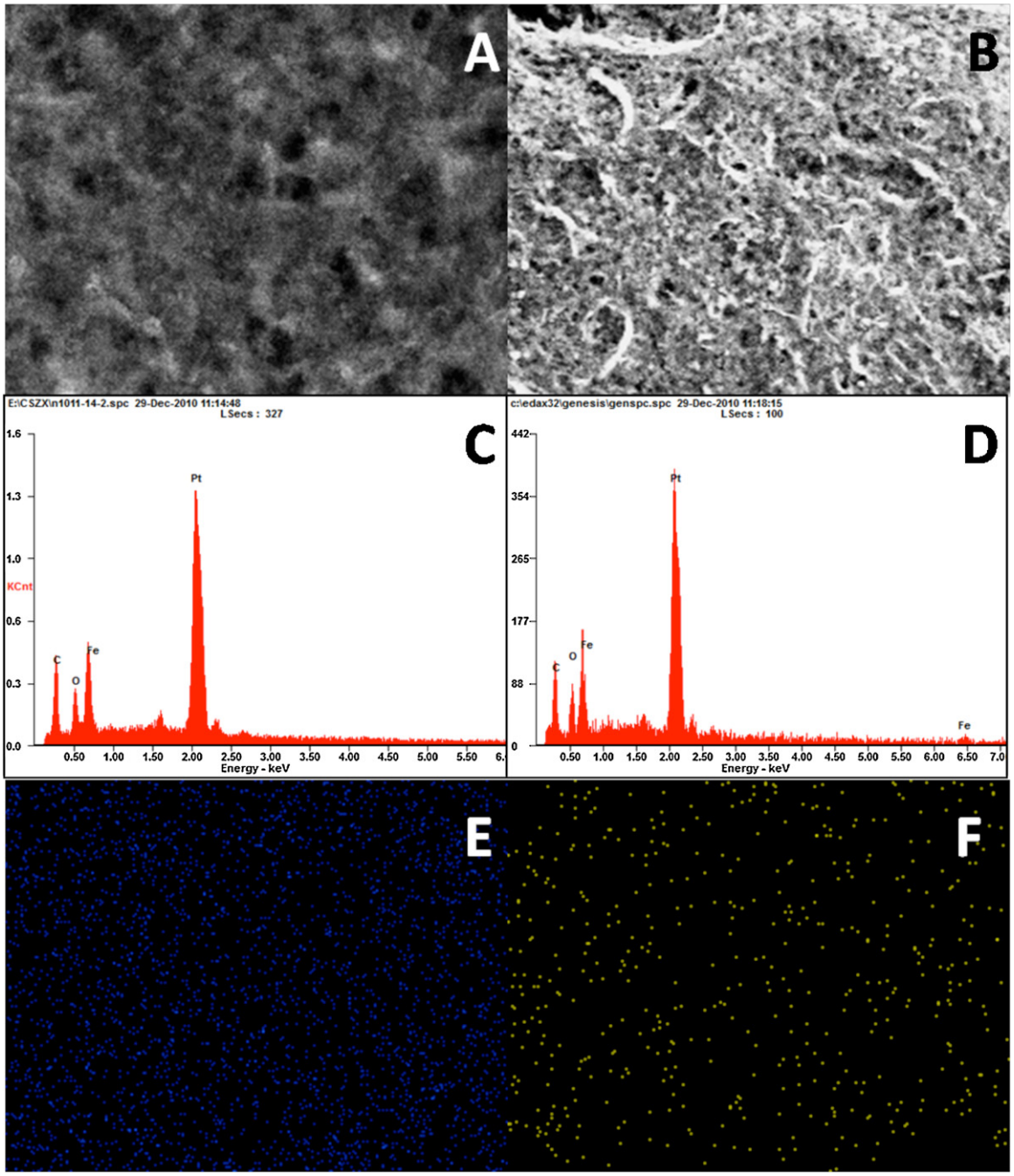

Fig. 6. EDS mapping of the surface of CCMs. (A) and (B) the selected-area for EDS (with and without PGS); (C) and (D) elemental qualitative analyses of the area (A) and (B); (E) and (F) the mapping of Fe element.

Fig. 3 shows the CV curves of Pt/C catalysts with different contents of PGS. The electrochemical specific active area (ECA) declines as the amount of PGS increases. Among them, the Pt/C with 5 wt% PGS (labeled as 5-PGS) and pristine Pt/C catalysts exhibit an ECA activity comparable, so that we chose the 5-PGS sample for further tests.

Fig. 4 illustrates Fe^{2+} ions crossover of the half CCMs with and without PGS. After 10 h, 378.3 $\mu g\,mL^{-1}$ Fe^{2+} pass through the half-CCM without PGS, while only 23.9 $\mu g\,mL^{-1}$ Fe^{2+} for that with 5% PGS. The crossover of Fe^{2+} arrives at the maximum value of 630.4 $\mu g\,mL^{-1}$ for the half-CCM without PGS, and 364 $\mu g\,mL^{-1}$ for that with PGS at 50 h. Afterwards the penetration capability of Fe^{2+} through the half-CCM becomes less and less due to the occupancy of the available exchange sites, leading to high resistance to transport subsequent Fe^{2+} ions. Evidently, the high specific surface area and the large CEC of PGS are responsible for the high absorption of Fe^{2+}, especially at the beginning.

SEM images of CCMs immersed in Fenton's reagent at 80 °C for 100 h and 200 h, respectively, are shown in Fig. 5. The microcrack occurs in catalyst layers during the treatment. The statistical width of cracks ranges from 1.5 to 9 μm, and their length distribution is between 12 and 160 μm in catalyst layers of the CCM-N (Fig. 5A) after 100 h. By contrast, the crack in the catalyst layer of the CCM-P only has a width of 5 μm at most and a max length of 50 μm (Fig. 5C). The thickness of catalyst layers is 7.6 μm and 10 μm for the CCM-N (Fig. 5B) and the CCM-P (Fig. 5D), respectively. Some newly created cracks can be observed on the surface of both CCMs. Such cracks further grow after 200 h treatment. The crack in

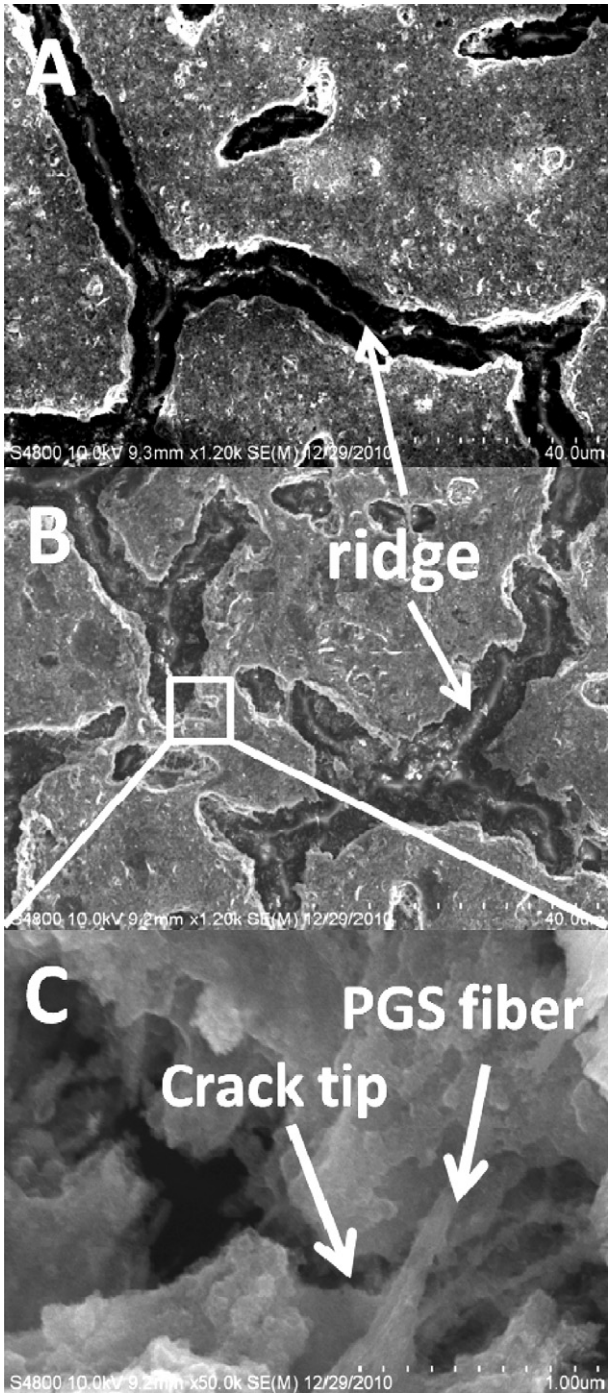

Fig. 7. HRSEM images of CCMs treated for 200 h. (A) CCM without PGS; (B) CCM with PGS; (C) a magnified area from (B).

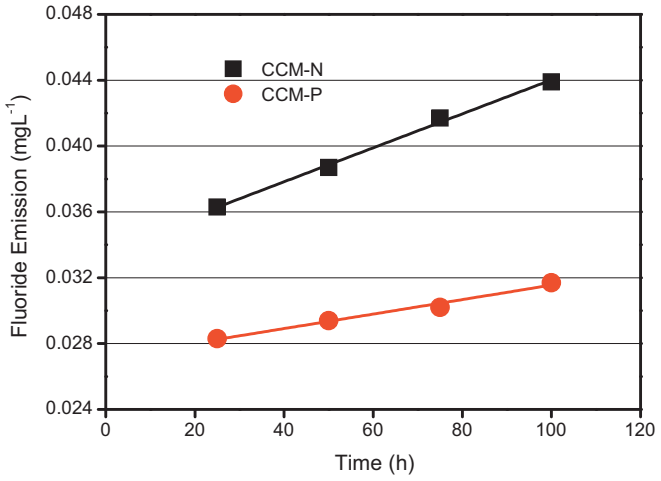

Fig. 8. Fluoride emissions of CCMs during treatment in Fenton's reagent.

catalyst layers of the CCM-N has a width of 4–20 μm and a length of 12–300 μm (Fig. 5E). In contrast, the width of cracks in catalyst layers of the CCM-P is in the range of 3–16 μm, and the length ranges from 8 to 91 μm (Fig. 5G). The thickness of catalyst layers is 5.8 and 8.6 μm for CCM-N and CCM-P, which is thinned by 1.8 and 1.4 μm for the CCM-N (Fig. 5F) and the CCM-P (Fig. 5H), respectively.

Fig. 6A and B is the selected-area for EDS analysis of the catalyst layer surface. No F element is detected on the surfaces of the treated CCMs (Fig. 6C and D), indicating that Nafion film on the surface of catalyst layers is attacked by OH radicals and completely decomposed. Fig. 6E and F shows the EDS mapping of Fe element. Although more Fe^{2+} ions present in catalyst layer with PGS as illustrated above (results from Fig. 4), less Fe is detected by EDS in comparison with that without PGS. We propose that most of Fe^{2+} ions might be absorbed in the channel of PGS and therefore could not be detected by EDS analysis. Fe^{2+} ions in the channels might lose the contact with H_2O_2, resulting in reduction of OH radicals according to Eq. (1), mitigating the attack toward Nafion which functions as binder and proton conductor. The carbon supported Pt catalyst detaches from catalyst layers when PFSA ionomer (Nafion) is attacked by OH radicals and decomposed, resulting in thinning of catalyst layers. Therefore, in the presence of catalyst layers, H_2O_2 predominantly damages the Nafion ionomer in catalyst layers.

The above result is strongly supported by high-resolution SEM observation as shown in Fig. 7. It is interesting that an ocean-ridge-like structure related to the PFSA ionomer degradation can be found on the uncovered surface of Nafion membrane in the middle of cracks (Fig. 7A and B). In these positions, we propose that H_2O_2 diffuses into the membrane without the catalyst layer as a protective layer, and then some fraction of H_2O_2 evaporates to form bubbles in the membrane [36] and constitutes the "ridge". The remaining H_2O_2 generates OH radicals and attacks the membrane. Fig. 7C clearly illustrates that PGS fibers successfully limit the growth of micro-cracks, confirming the reinforcing function of PGS to matrix. At the crack tip, the stress concentrating effect causes the growth of crack. PGS fibers lying at the crack tip can decelerate the rapid maturing of the crack, and the network constructed by "macromolecular comb" enhances the mechanical performance of catalyst layer before decomposition of the PFSA ionomer in catalyst layers [25].

Fig. 8 shows the fluoride emission from catalyst layers during 100 h treatment. The fluoride emission increases nearly linearly with the time. 0.0363 mg L^{-1} fluoride is released from CCM-N into the solution at 25 h, while only 0.0281 mg L^{-1} fluoride from CCM-P. Furthermore, 0.0439 and 0.0317 mg L^{-1} fluoride from CCM-N and CCM-P present in the solution at 100 h, respectively. The fitting line of CCM-N has a higher slope than that of CCM-P, indicating Nafion is decomposed at a higher rate in CCM-N. The test had to be stopped at 100 h, because afterwards the surface of Nafion membrane supporting catalyst layers is exposed in part to Fenton's reagent with the cracks increasing and then most of fluoride would predominantly origin from membrane while not from Nafion ionomer in catalyst layers, making the analysis difficult.

4. Conclusion

Palygorskite enhanced catalyst coated membranes (CCMs) possess a better chemical and mechanical stability against Fenton's

agent at 80 °C. Two contributions of palygorskite are responsible for the enhancement: one is the absorption of Fe^{2+} ions in the unique nano-channel of palygorskite significantly decreases the generation of OH radicals, the other is to retard crack growth by the reinforcing function of the palygorskite nanofiber. It is worth emphasizing that the concentration of H_2O_2 and Fe^{2+} introduced into the treatment is much higher than that generated under real fuel cell operation. Therefore we have reason to believe that the presence of such nano mineral fibers in catalyst layers can greatly improve the durability of membrane electrode assembly (MEA) for polymer electrolyte membrane fuel cells.

Acknowledgments

This work was supported by the National Natural Science Foundation of China (NSFC) (50972112), the Major State Basic Research Development Program of China (973 Program) (No. 2012CB215504), the Fundamental Research Funds for the Central Universities and the Self-determined and Innovative Research Funds of WUT (2010-JL-01).

References

[1] S.S. Zhang, X.Z. Yuan, H.J. Wang, W. Mérida, H. Zhu, J. Shen, et al., Int. J. Hydrogen Energy 34 (2009) 388–404.
[2] Y.Y. Shao, J. Wang, R. Kou, M. Engelhard, J. Liu, Y.H. Lin, et al., Electrochim. Acta 54 (2009) 3109.
[3] S. Maass, F. Finsterwalder, G. Frank, R. Hartmann, C. Merten, J. Power Sources 176 (2008) 444.
[4] C.V. Subban, Q. Zhou, A. Hu, T.E. Moylan, F.T. Wagner, F.J. Disalvo, J. Am. Chem. Soc. 132 (2010) 17531.
[5] D.E. Curtin, R.D. Lousenberg, T.J. Henry, P.C. Tangeman, M.E. Tisack, J. Power Sources 131 (2004) 41–48.
[6] C. Walling, J. Accounts Chem. Res. 8 (1975) 125.
[7] X.Y. Huang, R. Solasi, Y. Zou, M. Feshiler, K. Reifsnider, D. Condit, et al., J. Polym. Sci. Polym. Phys. 44 (2006) 2346.
[8] F. Rong, C. Huang, Z.S. Liu, D.T. Song, Q.P. Wang, J. Power Sources 175 (2008) 699.
[9] S.C. Mu, P. Zhao, C. Xu, Y. Gao, M. Pan, Int. J. Hydrogen Energy 35 (2010) 8155.
[10] S.C. Mu, C. Xu, P. Zhao, H.L. Tang, M. Pan, Int. J. Hydrogen Energy 35 (2010) 2872.
[11] J. Xie, D.L. Wood, D.M. Wayne, T.A. Zawodzinski, P. Atanassov, R.L. Borup, J. Electrochem. Soc. 152 (2005) A104.
[12] B. Xu, W.M. Huang, Y.T. Pei, Z.G. Chen, A. Kraft, R. Reuben, et al., Eur. Polym. J. 45 (2009) 1904.
[13] S.Q. Xue, M. Reinholdt, T.J. Pinnavaia, J. Polym. 47 (2006) 3344–3350.
[14] S.C. Mu, M. Pan, R.Z. Yuan, Mater. Sci. Forum 475 (2005) 2441.
[15] S.Q. Xue, M. Reinholdt, T.J. Pinnavaia, Polymer 47 (2006) 3344.
[16] D.J. Lapparent, Compt. Rend. 201 (1935) 481.
[17] H.H. Murrary, Appl. Clay Sci. 17 (2000) 207.
[18] E.V. George, J.S. Carlos, L.A. James, Am. Mineral. 64 (1979) 215.
[19] G. Chiari, R. Giustetto, G. Ricchiardi, Eur. J. Mineral. 15 (2003) 21.
[20] R. Giustetto, F.X.L. Xamena, G. Ricchiardi, S. Bordiga, A. Damin, R. Gobetto, M.R. Chierotti, J. Phys. Chem. B 109 (2005) 19360.
[21] Q.H. Fan, Z. Li, H.G.Z. Zhao, H. Jia, J.Z. Xu, W.S. Wu, Appl. Clay Sci. 45 (2009) 111.
[22] M. Shirvani, H. Shaiatmadari, M. Kalbasi, F. Nourbakhsh, B. Najafi, Colloids Surf. A 287 (2006) 182.
[23] W.S. Wu, Q.H. Fan, J.Z. Xu, Z.W. Niu, S.S. Lu, Appl. Radiat. Isot. 65 (2007) 1108.
[24] Q.H. Fan, W.S. Wu, X.P. Song, J.Z. Xu, J. Hu, Z.W. Niu, Radiochim. Acta 96 (2008) 159.
[25] F. Xu, S.C. Mu, M. Pan, J. Membr. Sci. (2011), doi:10.1016/j.memsci.2011.04.027.
[26] H. Chen, Y.G. Zhao, A.Q. Wang, J. Hazard. Mater. 149 (2007) 346.
[27] J.H. Potgieter, S.S. Potgieter-Vermaak, P.D. Kalibantonga, J. Miner. Eng. 19 (2006) 463.
[28] C. Yuanfeng, X. Jiyue, P. Yuguan, Acta Mineral. Sin. 28 (2008) 343.
[29] A. Pozio, R.F. Silva, M. De Francesco, L. Giorgi, Electrochim. Acta 48 (2003) 1543.
[30] P. Maletzky, R. Bauer, Chemosphere 38 (1999) 2315.
[31] T.J. Peckham, S. Holdcroft, Adv. Mater. 22 (2010) 4667.
[32] V.R. Albertini, B. Paci, F. Nobili, R. Marassi, M.D. Michiel, Adv. Mater. 21 (2009) 578.
[33] M. Lopez, B. Kipling, H.L. Yeager, Anal. Chem. 49 (1977) 629.
[34] K. Mauritz, S.R. Lowry, Polym. Prep. Am. Chem. Soc. Div. Polym. Chem. 19 (1978) 336.
[35] T. Okada, G. Xie, O. Gorseth, S. Kjelstrup, N. Nakamura, T. Arimura, Electrochim. Acta 43 (1998) 3741.
[36] H.L. Tang, P.K. Shen, S.P. Jiang, F. Wang, M. Pan, J. Power Sources 170 (2007) 85.